3D CFD Modeling Investigation of Potential Vortex Formation at the Intakes of Caruachi Powerhouse

A. Marcano
C.V.G. EDELCA Dept. of Hydraulics, San Felix, Estado Bolívar, Venezuela

L. Rojas-Solórzano
Associate Profesor. Dept. of Energy Conversion, Universidad Simón Bolívar, Venezuela

M. Reyes
Associate Professor. Dept. of Thermodynamics, Universidad Simón Bolívar, Venezuela

ABSTRACT: In this paper, the 3-D CFD simulation of the free-surface flow approaching the intakes of Caruachi Powerhouse is presented. The aim of the investigation is to determine whether or not vortex structures are likely to appear from the water surface through the intakes, as the result of the presence of cofferdams placed few meters upstream of the intakes. The presence of cofferdams was a note of concern with regard to the effects they might have on the turbine intakes once the hydroelectric central starts operating. In all the considered conditions, results did not show neither strong surface vortices in the proximities of the Power House intakes, nor air entrainment-entrapment towards the intakes, which reflects the safe operation of the turbines in the presence of the cofferdams. The latter added in decision taking on leaving the cofferdams submerged instead of removing them, which resulted in cost savings for the project.

1 CARUACHI PROJECT AND CARONI RIVER DIVERSION

The Caruachi project located on the Caroni River at Southeastern Venezuela will add 2.196 MW up to the national electricity market. The power plant, equipped with 12 Kaplan units and a 30.000 m^3/s capacity spillway, is located 59 Km downstream of Guri Dam and 25 Km upstream of Macagua Dam, and conforms together with Tocoma Dam, the Lower Caroni Hydroelectric Development. During the first stage of construction of Caruachi Project, a 3 Km-long cofferdams, named Cofferdam 'A' and Cofferdam 'B', hereafter, made of rock fill and concrete, respectively were built few meters upstream the turbine intakes to allow construction of the main structures in the dry (i.e., spillway, power house, intakes, gravity dams, etc.). The river was diverted from its natural path, within a channel 350 meters width, in its left bank, to allow a maximum flowrate of 13.000 m^3/s, regulated at Guri reservoir while Caruachi Project construction was ongoing. During the second stage of construction, the river was diverted through 18, 5,5X9m bottom sluices left in the spillway lower body, to allow the left embankment dam to be erected. Following the sluice closure on December, 2002 the reservoir was filled and, two generating units have been commissioned since April 2003. Construction schedule contemplates commercial operation of the last unit in early 2006.

Normally, cofferdams are built as temporary structures and they should be removed at least partially, after they fulfilled their purpose of keeping construction areas in the dry. However, removing cofferdams built on large rivers is complex and might result uneconomical. For this reason, due consideration should be given to either removing or leaving them submerged, provided hydraulic flow behavior is acceptable i.e., avoiding additional energy loses and/or malfunctioning of the operating units because of undesirable swirling flow at intakes, vortex formation, and flow separation. At Caruachi Project the presence of Cofferdams 'A' and 'B' was a note of concern regarding to the effects they might have on the turbine intakes once the hydroelectric central starts operation. In this paper, results of a 3 Dimensional CFD numerical model that was set up to investigate potential vortex formation at the intakes of Caruachi units, due to the presence of the Cofferdams "A" and "B", are presented.

2 CFD ANALYSIS OF THE PROBLEM

The detailed calculation of the fluid motion within a complex geometry is a very difficult task from the analytical point of view, since the simultaneous solution of momentum, continuity and sometimes energy governing equations is required under boundary and initial conditions which many times are as complex as the geometry itself. During the last years it has been demonstrated that many complex problems may be satisfactorily solved through finite difference, finite element, finite control volume and other discretization techniques.

CFD is a computational technique for the numerical solution of the time and spatially discrete fluid mechanics governing equations. In this work, CFX4.3TM is used as the base open CFD code, which is designed and validated for computing the flow field by using the finite control volume technique.

2.1 *Numerical Issues*

The numerical method works by dividing the physical region into a large number of control volumes (AEA Technology, 1997). The set of differential governing equations are written as algebraic equations within each of those control volumes, after applying finite differences to relate the pressure, velocity and other variables (e.g., volumetric fraction) with values in neighbor volumes. The solution to the problem consists in the solution of a non-linear system of algebraic equations.

The control volume method divides the domain in a large number of control volumes with a central node and, in general, it is connected to neighboring control volumes.

All the terms in the governing equations, except the convective term, are spatially discretized using second order central differences. A hybrid scheme is used to discretize the convective term. The non-linear nature of the governing equations leads to an iterative solution procedure of the system of equations. The pressure term is dealt as a source term in the momentum equation and the SIMPLEC (Patankar, 1983) algorithm is used to couple the mass and momentum equations. This semi-implicit algorithm solves the continuity equation through a pressure correction term for the velocity components. Further details are presented in the next sections.

2.2 *Free Surface Air-Water Modeling*

To model the air-water segregated flow, the mass conservation of each phase is solved as one of the set of governing equations, while the momentum equation (Navier-Stokes equation since the fluids are Newtonian) for each phase are added up to get rid of the interphase momentum transfer. There is a closure equation for the volume fraction, which states that both phases volume fraction must add up to one at every fluid location.

Furthermore, both the Navier-Stokes and continuity equations are the governing equations, no matter the flow is in laminar or turbulent regime. However, the size of the mesh and time stepping would make it prohibitive to solve the smallest time- and length-scales in today's computers. Therefore, the turbulence is modeled using the Reynolds Averaged Navier-Stokes (RANS) and mass equations and the two-equation model based on the turbulent viscosity and the turbulent kinetic energy 'k' and turbulent dissipation 'ε', named the k- ε model with wall functions (AEA Technology, 1997). The k-ε model has proven effectiveness in solving industrial problems.

The multiphase model considers the possibility of air-water mixture, at a larger scale than molecular, while still at smaller scale than what being solved for. This is, each phase is treated as an inter-penetrating continuum, which implies that each phase may be present in every control volume and, the phase volume fraction is equal to the fraction of volume occupied. Therefore, the problem is solved in an Eulerian-Eulerian frame of reference for the two phases, even though the intrinsic volumetric forces (e.g., gravity) will determine, through mass conservation, the solely existence, co-existence or non-existence of a single phase.

Both phases are considered to be incompressible and isothermal.

Therefore, the governing equations are presented, indicating with the sub-index each phase, as follows:

Mass Conservation:

$$\nabla \bullet \left(r_\alpha \rho_\alpha U_\alpha\right) = 0 \tag{1}$$

Linear Momentum:

$$\frac{\partial}{\partial t}(\rho U) + \nabla \bullet \left(\left(\rho U \otimes U - \mu\left(\nabla U + (\nabla U)^T\right)\right)\right) = \left(B - \nabla p\right) \tag{2}$$

In eqn. (2), the left-hand-side terms represent the transport of convective and diffusive momentum. The right-hand-side term represents the body and pressure forces.
Furthermore, in this equation:

$$U_\alpha = U_\beta = U \tag{3}$$

$$p_\alpha = p_\beta = p \tag{4}$$

$$\rho = \sum_{\alpha=1}^{2} r_\alpha \rho_\alpha \tag{5}$$

$$\mu = \sum_{\alpha=1}^{Np} r_\alpha \mu_\alpha \tag{6}$$

And the algebraic restriction for the addition all volume fractions at each control volume:

$$\sum_{\alpha=1} r_\alpha = 1 \tag{7}$$

The multiphase model here proposed has proven to give a good approximation (i.e., CRS4 Technical Report 99/20, 1999) when the gravity force trends to stratify the phases as in free surface flows. In this case, the volume fractions are equal to 1 or 0 everywhere, except at the interphase, which makes it reasonable to have a unique velocity field for both phases.

2.3 *Interphase Refinement Algorithm*

During the simulation convergence iterative process, the water and air, initially mixed, tend to segregate due to their differences in density, creating homogeneous volume fraction fields for each phase, equal to 0 or to 1, such that it suddenly changes at the two-fluid interphase. To avoid a blurry interphase caused by numerical diffusion of the volumetric fraction equations (mass conservation for each phase), a refinement algorithm is used. This surface contouring algorithm requires a local fine mesh and therefore a proficient user-analyst.
In detail, the algorithm adjusts the volumetric fraction of the fluids at the interphase for each iteration. The interphase is defined as the surface in which volume fraction for both fluids, r_1 and r_2, are equal to 0.5 each. Firstly, the program identifies the control volumes at the interphase, by checking whether or not r_1-0.5 for certain control volume changes sign with respect to its neighbors. Then, the program identifies the fluid on the wrong side of the interphase and translates it to the right side, ensuring the volume conservation. During this procedure, all the interphase volumes are fixed.

2.4 *Turbulent Model*

The two-equation model used in these simulations is the standard k-ε with wall functions for dampening the turbulent viscosity near the walls. The equations of the model are:

Transport of Turbulent Kinetic Energy k :

$$\nabla \bullet \left(r_\alpha \left(\rho_\alpha U_\alpha k_\alpha - \left(\mu + \frac{\mu_{T\alpha}}{\sigma_k} \right) \nabla k_\alpha \right) \right) = r_\alpha S_{k\alpha} \tag{8}$$

Transport of the Dissipation Rate of Turbulent Kinetic Energy ε :

$$\nabla \bullet \left(r_\alpha \left(\rho_\alpha U_\alpha \varepsilon_\alpha - \left(\mu + \frac{\mu_{T\alpha}}{\sigma_\varepsilon} \right) \nabla \varepsilon_\alpha \right) \right) = r_\alpha S_{\varepsilon\alpha} \tag{9}$$

Where the respective source terms are given by:

$$S_{k\alpha} = P_\alpha + G_\alpha - \rho_\alpha \varepsilon_\alpha \tag{10}$$

$$S_{\varepsilon\alpha} = \frac{\varepsilon_\alpha}{k_\alpha}\left(C_{1\varepsilon}\left(P_\alpha + C_{3\varepsilon} max\left(G_\alpha, 0\right)\right) - C_{2\varepsilon}\rho_\alpha\varepsilon_\alpha\right) \quad (11)$$

The turbulent viscosity is calculated through the Prandtl-Kolmogorov relationship:

$$\mu_{T\alpha} = C_\mu \rho_\alpha \frac{k_\alpha^2}{\varepsilon_\alpha} \quad (12)$$

and the empirical coefficients (taken for free turbulence cases) given by: C_μ=0.09; C_1=1.44; C_2=1.92; C_3=0.0; and C_k=0.4187.

3 DISCRETIZATION OF THE GOVERNING EQUATIONS

The differential expressions of the several terms in the governing equations are integrated within each control volume, and the discrete treatment of the derivatives is performed by using finite differences, otherwise known as the finite volume method, with all variables defined at the center of the control volumes in the domain. The resulting discrete set of equations reflects the connection of the volume center and its neighbor volume centers. All equations, except by the mass conservation have a similar general layout:

$$\frac{\partial(\rho\phi)}{\partial t} + \nabla.\left(\rho U\phi\right) - \nabla.\left(\Gamma\nabla\phi\right) = S \quad (13)$$

Where, Γ is the effective diffusivity (laminar + turbulent) for the transport of the intensive property given by (velocity or specific energy, for instance, for the momentum and energy equations, respectively). When eqn. (13) is integrated within the control volume, it leads to:

$$\int \frac{\partial(\rho\phi)}{\partial t} dV + \int \rho\phi U.ndA - \int \Gamma\nabla\phi.ndA = \int S dV \quad (14)$$

All terms, in all equations are discretized using second order central differences, but the advective term and its coefficients which are determined using the Rie-Chow algorithm (see AEA Technology, 1997). In particular, the advective term is treated using the Hybrid (Upwind/Central differences) method, named HDS, which is robust and accurate.

4 NUMERICAL SIMULATIONS

After developing a preliminary 2-D and 3-D model to adjust the appropriate mesh refinement, boundary and initial conditions in an economical time-frame, the final 3-D model considered the most important details of the civil structures, since they are a very important part to be considered in the study.

Details of the actual structure are shown in Figs. 1 and 2. The main dam is integrated to the Power House and the dam is 55 m height and 360 m long. There are 12 Kaplan turbo-generator units mounted onto a structure 60 m long. The spillway is 178.16 m long and overflow section is at 70.55 m.a.s.l. The CFRD left Dam is 900 m long and 50 m height, while the left embankment dam is 4.200 m long and 45 m height, both connected to the main concrete dam structure.

Once the project is finished, normal pool elevation will be 91,25 m.a.s.l. After studying photographs, bathymetric surveys drawings of the river bed and the actual prototype site, a final 3-D model geometry was developed resulting in a mesh with more than 100.000 elements (Figures 3 to 5).

The computational equipment used for the simulations (both 2-D and 3-D) was an Intel Pentium IV PC / 1,7 GHz CPU clock speed / 400 MHz bus speed / 512 MB Ram / 64 MB SDRam video memory, with the following characteristic convergence performance:

a.2-D introductory case: 4–6 hours per case

b.3-D case: Preliminary/12-15 hours per case; Final/24-36 hours per case

Fig. 1. Aerial Photograph of Caruachi Power-house and Civil Works

Fig. 2. Aerial Photograph of Caruachi Dam (Abutment details)

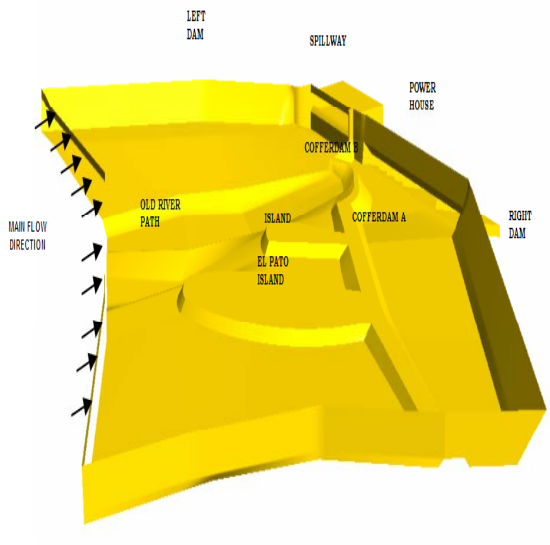

Fig. 3. 3-D Geometric Model

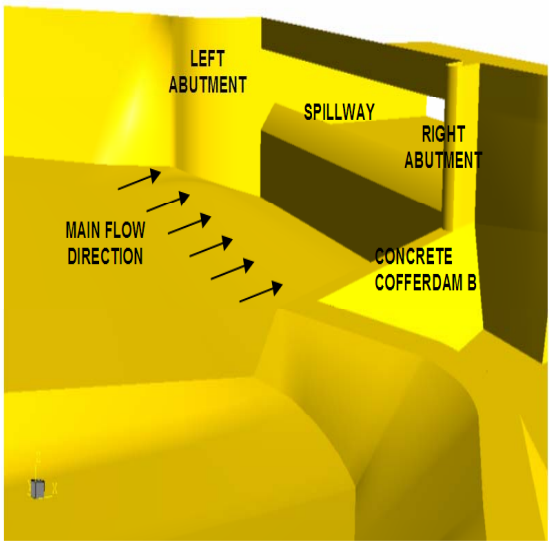

Fig. 4. Abutment Details in 3-D Model

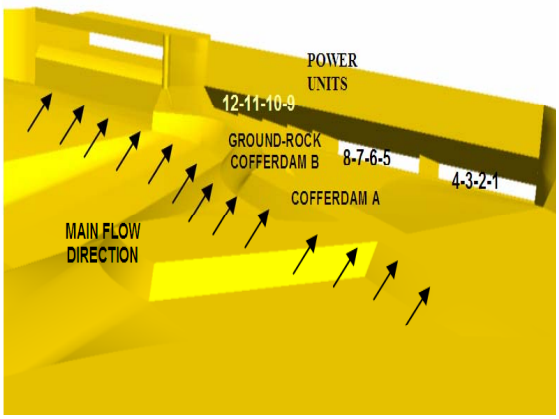

Fig. 5. Power House Detail in 3-D Model

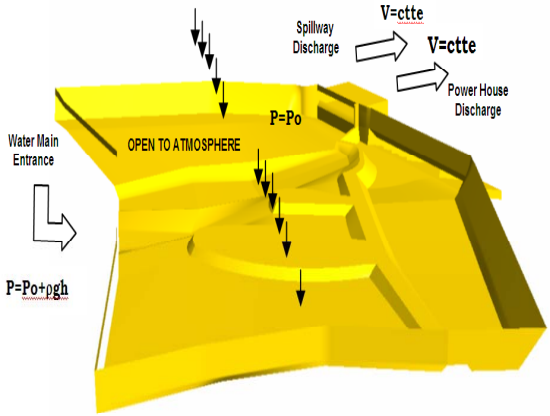

Fig. 6. Boundary Conditions

5 BOUNDARY AND INITIAL CONDITIONS

The simulations consider the river upstream level under different Spillway and Power House operating conditions. The level of the river is preset via a hydrostatic pressure gradient at the entrance, while an amount of water flow is withdrawn through the machines and the Spillway via a uniform velocity profile. The roof of the geometry was declared open to the free flow of air (Fig. 6). The initial condition corresponds to a homogeneous mixture of water-air at rest within the whole domain, and then perturbed by the boundary conditions at t=0+.

6 CASES SIMULATED

During the simulations, six flow conditions/cases were explored: (I) Maximum infrequent river-level (92.40 m.a.s.l.), flow of 5000 m^3/s through all Powerhouse units, flow of 25000 m^3/s through the spillway; (II) Maximum infrequent river-level (92.40 m.a.s.l.), flow of 5000 m^3/s through all Powerhouse units, flow of 25000 m^3/s through the Spillway, but no cofferdams present, for comparison purposes with the most critical condition resulted from the cofferdam-existing simulation; (III) Minimum infrequent river-level (88.55 meters above sea level 'm.a.s.l.'), flow of 550 m^3/s only through Unit 12, flow of 4450 m^3/s through the Spillway; (IV) Minimum infrequent river-level (88.55 m.a.s.l.), flow of 550 m^3/s only through Unit 9, flow of 4450 m^3/s through the spillway; (V) Maximum normal river-level (91.25 m.a.s.l.), flow of 5000 m^3/s through all Powerhouse units, no flow through the spillway; (VI) Maximum normal river-level (90.25 m.a.s.l.), flow of 5000 m^3/s through all Powerhouse units, no flow through the Spillway. For space limitations in this paper, only cases I and II will be discussed. Further details of the computational field space are shown in Fig. 7.

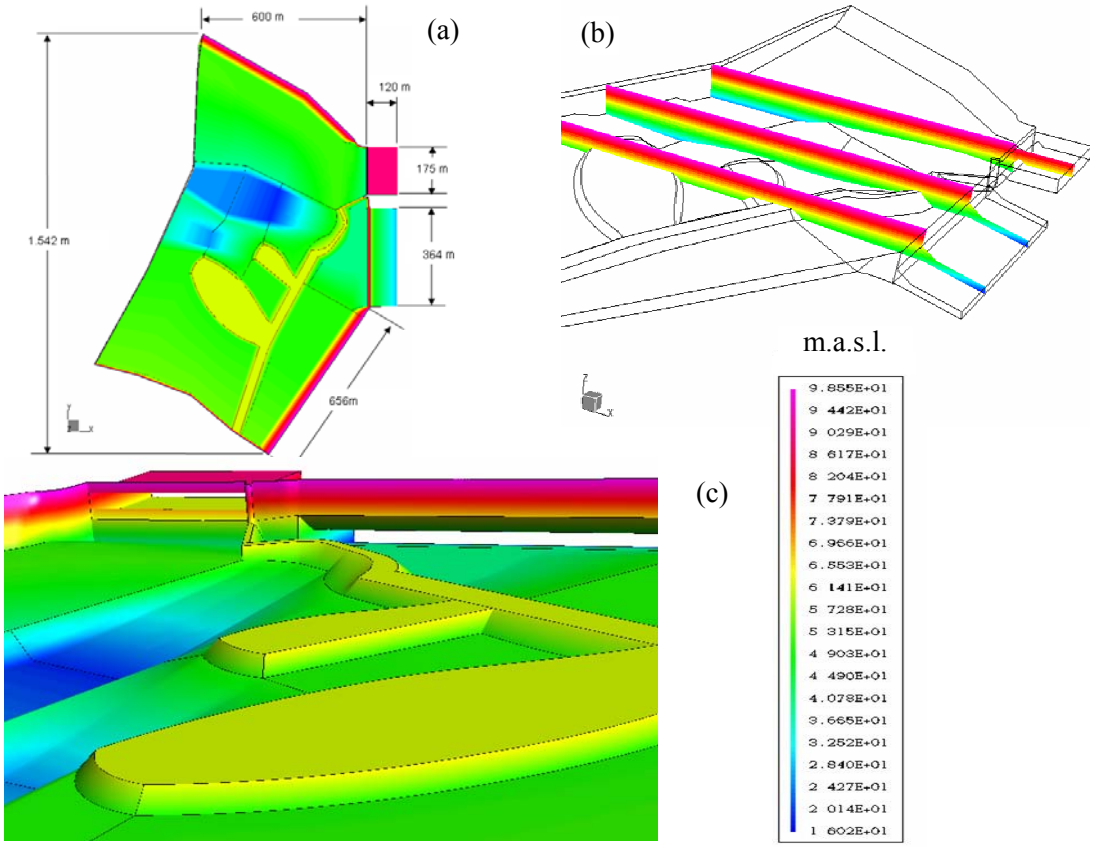

Fig.7. Surface Details with Levels of the Computational Model with Cofferdams. (a) Upper view with approximate dimensions. (b) Side view. (c) Perspective view of power house and spillway.

7 EFFECTS CAUSED BY COFFERDAMS ‘A’ AND ‘B’

Figures 8-11 depict a comparison between conditions with and without Cofferdams ‘A’ and ‘B’, named cases I and II, respectively. Both cases are shown for the maximum infrequent river level of 92.4 m.a.s.l. and flowrate of 5000 m3/s through the entire Power House and 25.000 m3/s through the Spillway.

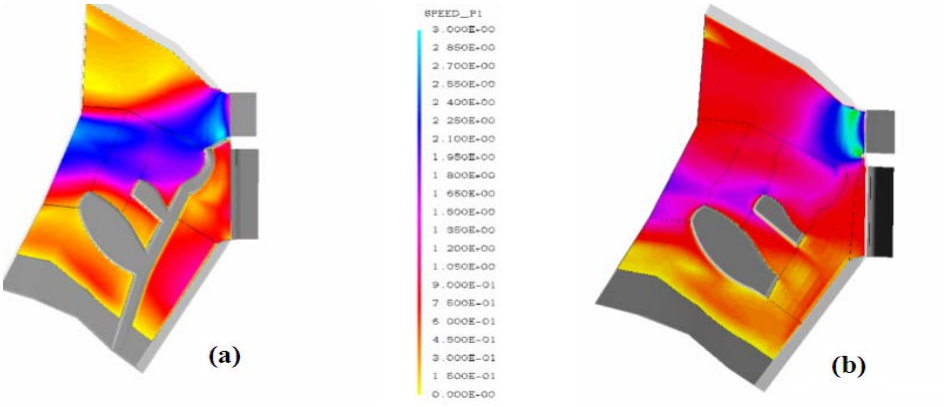

Fig. 8. Velocity Field (speed) contour plot at 53 m.a.s.l.: (a) Case I, (b) Case II

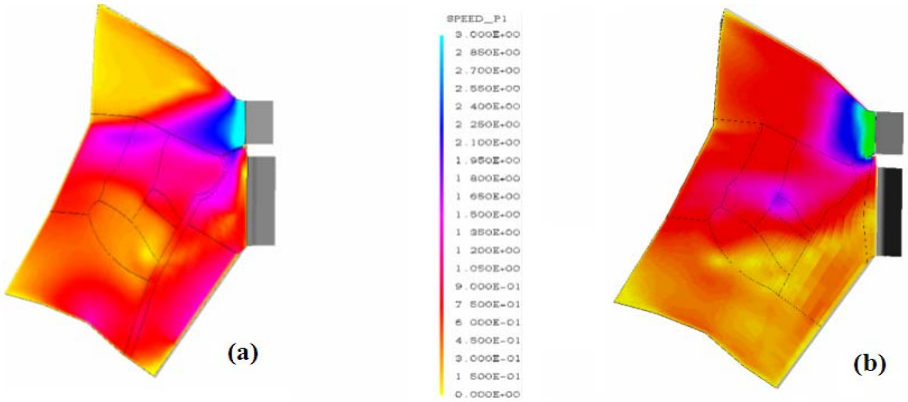

Fig. 9. Velocity Field (speed) contour plot at 89.4 m.a.s.l.: (a) Case I, (b) Case II

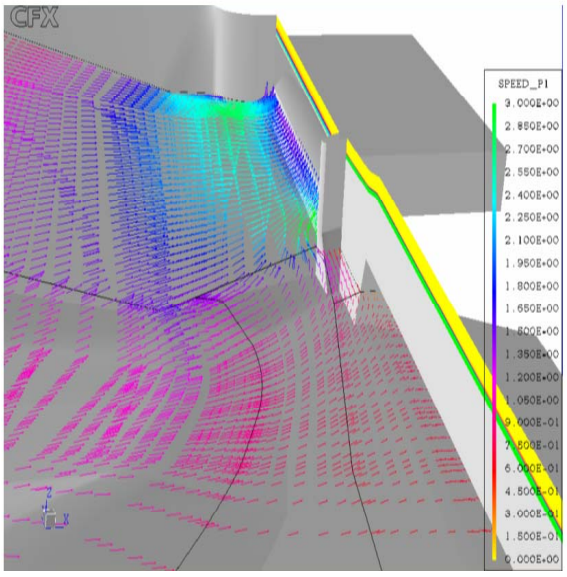

Fig. 10. Case II (with cofferdams): Velocity Field and Speed at 54 m.a.s.l.

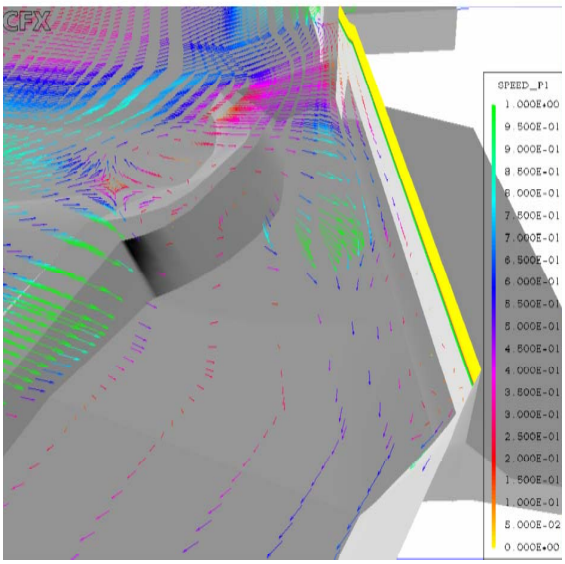

Fig. 11. Caso III (with cofferdams): Velocity Field and Speed at 88.55 m.a.s.l. (free surface)

Fig. 8 shows a velocity contour plot at 40 meters under the free surface (i.e., 7 meters under the cofferdam top for case I). It is clearly depicted that the presence of the cofferdams does not affect the uniform distribution of flow approaching the Power House and Spillway. Moreover, the cofferdam (case II) favors a large volume of the watercourse through the original river path and left sideways of the present islands. Even more, in Fig. 9, at 3 meters under the free surface, there are no noticeable differences between cases I and II, at the dam vicinity.
Fig. 10 shows the well-behaved flow field above the cofferdam at 54 m.a.s.l. It is appreciated the larger velocities at the Spillway entrance, and a uniform velocity approaching the Power House intakes, with no signs of vortex formation.
Fig. 11 depicts the velocity field at the free surface, nearby the Power House for case III (i.e., 88.55 m.a.s.l. river level, with Unit 12 in stand-alone operation and 4450 m3/s through the Spillway. This was the only case in which vortices (2 of them), though weak, were observed. At lower depths (not shown in this paper), no signs of vortices were observed, indicating that these vortices responded to the natural superficial flow re-orientation of the large volume of water impacting the dam.

8 CONCLUDING REMARKS

This paper presents the numerical simulation of the flow approaching the Caruachi Dam when Cofferdams 'A' and 'B' are present. Results lead to the following conclusions:
No surface vortices were observed in the vicinity of the Power House when the cofferdams 'A' and 'B' were present. Therefore, for the supposed flow conditions, air entrainment towards the power units is discarded, i.e., cofferdams 'A' and 'B' are not likely to affect significantly the operation of power units, under the conditions here considered.

REFERENCES

AEA Technology Engineering Software, Inc., CFX-4.3, "Solver Manual", (1997)

Casey M. and Wintergerste, T., "Special Interest Group on Quality and Trust in Industrial CFD: Best Practice Guidelines", European Research Community on Flow, Turbulence and Combustion (ERCOFTAC), Version 1.0, January 2000.

Consulta Internet: http://www.aeat.com.

Consulta Internet: http://www.cfdtech.com.

CRS4 Technical Report 99/20, "Simulation of the Free Surface Flow inside a Rotating Cylinder", http://www.crs4.it/~cfdea/LMfreesurf/rotcyl.html, 1999.

Hubred G., Mason A., Parks S. and Petty Ch., "Dispersed Phase Separations: Can CFD Help?." ETCE 2000/OMAE2000 Conference. New Orleans, LA. Feb.2000.

Patankar, S. and Spalding, D., "A Calculation Procedure for Heat, Mass and Momentum Transfer in Three Dimensional Parabolic Flows", Int. Journal of Heat and Mass Transfer, 15p-1787, 1972.

Patankar, S., "Numerical Heat Transfer and Fluid Flow", Ed. Hemisphere, New York (1983).

Rhie, C. and Chow, W., "Numerical Study of the Turbulent Flow Past an Airfoil with Trailing Edge Separation", AIAA J1, 21 pp, 1527-1532, 1983.

Streeter V. y Wylie B., "Mecánica de Fluidos". Sexta Edición. 1979.

Van Doormal, J. and Raithby, G., "Enhancements of the SIMPLE Method for Predicting Incompressible Fluid Flows", Numerical Heat Transfer, 7 pp, 147-163, 1984.

White, F.M., "Viscous Fluid Flow". 1989.